

Moiré Butterflies

R. Bistritzer* and A.H. MacDonald¹

¹*Department of Physics, The University of Texas at Austin, Austin Texas 78712 USA*

**rafib@physics.utexas.edu*

(Dated: November 26, 2024)

The Hofstadter butterfly spectral patterns of lattice electrons in an external magnetic field yield some of the most beguiling images in physics[1–7]. In this Letter we explore the magneto-electronic spectra of systems with moiré spatial patterns[8], concentrating on the case of twisted bilayer graphene. Because long-period spatial patterns are accurately formed at small twist angles, fractal *butterfly* spectra and associated magneto-transport and magneto-mechanical anomalies emerge at accessible magnetic field strengths.

The fractal Hofstadter spectrum is a canonical example of electronic structure in a system with incommensurate length scales, and has fascinated physicists and mathematicians for over a half a century. The classic butterfly pattern is formed by the magnetic field dependent support of the eigenvalue spectrum of the Schrodinger equation for a near-neighbor hopping model on a square lattice. Similar but distinct[9] patterns describe the magneto-spectrum of any two-dimensional (2D) system of Bloch electrons.

Quite generally magneto-Bloch Hamiltonians are block diagonalizable only when the magnetic flux through a 2D unit cell Φ is a rational multiple of the magnetic flux quantum Φ_0 . For $\alpha \equiv \Phi_0/\Phi = p/q$ the spectrum consists of continuous subbands each containing an areal density of $B/q\Phi_0$, q times smaller than the usual semiclassical Landau level density. Because the x and y components of cyclotron orbit centers are canonically conjugate in a magnetic field[10], smearing the periodic potential over the magnetic length scale $\ell = (\Phi_0/2\pi B)^{1/2}$, the fractal pattern of gaps within Landau levels becomes visible only when α is not too much larger than one. For atomic periodicity this condition is not met until the magnetic field strength exceeds laboratory scales by a factor of about one thousand. In moiré systems, however, the pattern period is inversely proportional to the twist angle and can easily exceed ℓ . Graphene moiré systems realize Hofstadter physics at fields of a few Tesla, without recourse to the difficult and potentially damaging photolithographic patterning used previously [11] to realize Hofstadter physics in the lab.

Because of the relatively weak forces between adjacent graphene layers, double layer graphene systems with a

variety of different stacking sequences occur in bulk graphite[12], epitaxially grown multi-layer graphene[13], and in mechanically exfoliated multilayers [14]. Relative twists between layers can also be created by folding a single layer[15, 16]. The stacking arrangement in a two-layer system can be characterized by the twist angle θ , and by a relative translation \mathbf{d} . Different electronic structure aspects of the twisted bilayer have captured theoretical attention[17–23], and have already spurred some experimental observations[14, 24].

For θ smaller than roughly ten degrees, the low energy spectrum is faithfully described by a continuum model obtained via an envelope function approximation[17, 23]. For small twist angles, this model shows that it is meaningful to describe the electronic structure in terms of Bloch bands for any θ despite the fact that the atomic network is periodic only for a discrete set of angles. The Bloch bands in this description are intimately related to the moiré pattern clearly observed in scanning tunneling microscopy measurements[13]. The moiré period for bilayer graphene is $D = a/[\sin(\theta/2)]$ where a is graphene’s lattice constant. Because a translation of one layer with respect to the other only shifts the moiré pattern the electronic structure is virtually independent of \mathbf{d} [23] except at large commensurate twist angles. In what follows, we therefore set \mathbf{d} to zero.

The continuum limit of a π -band tight-binding model for the twisted bilayer yields a transparent physical picture in which Dirac cones are coupled by a position and sub-lattice dependent interlayer hopping $T(\mathbf{r})$ operator that captures the local coordination of the twisted honeycomb lattices. It is $T(\mathbf{r})$, and not a periodic potential, which is responsible for the moiré butterfly. Because the moiré unit cell area $\Omega_M \propto \theta^{-2}$ (see Supplementary Information), the flux through a moiré unit cell increases rapidly as the twist angle is reduced. As in the periodic potential case, gaps open within Landau levels for $\alpha \lesssim 1$. Because $B[T] \approx 4(\theta^\circ)^2/\alpha$, significant splitting of the isolated layers Dirac Landau levels appear already at low magnetic fields for small θ .

In the absence of inter-layer coupling, the spectrum consists of degenerate Dirac Landau-levels at energies $\pm\omega_c\sqrt{n}$, where $\omega_c = \sqrt{2}v/\ell$ is the cyclotron energy, and v is the graphene sheet Dirac velocity. Because of the layer degeneracy, gaps between Landau levels produce quantum Hall effects at odd, rather than half odd[25], integer filling factors. (Spin and valley degeneracy are left implicit throughout this article.) Coupling between the layers splits the Landau levels in both layers into q sub-bands and couples them together as illustrated in Fig.1 for the $\theta = 2^\circ$ case. It is clear that interlayer coupling at strong fields completely alters the spectrum.

We now briefly derive the equations we use to evaluate the moiré butterfly spectrum at rational values of α , present numerical results for a typical twist angle, and discuss the magneto-transport and magneto-mechanical anomalies that

they imply.

The low energy electronic structure of a twisted bilayer is well captured by the continuum model in which[23]

$$H = \begin{pmatrix} h(-\theta/2) & T(\mathbf{r}) \\ T^\dagger(\mathbf{r}) & h(\theta/2) \end{pmatrix} \quad (1)$$

where $h = iv\sigma \cdot \nabla$ with $\sigma = (\sigma_x, \sigma_y)$ being the sub-lattice Pauli matrices of the single-layer graphene Hamiltonian, and

$$T(\mathbf{r}) = w \sum_j e^{-i\mathbf{q}_j \cdot \mathbf{r}} T_j \quad (2)$$

is the inter-layer hopping matrix. Here

$$T_1 = \begin{pmatrix} 1 & 1 \\ 1 & 1 \end{pmatrix}, T_2 = \begin{pmatrix} e^{-i\phi} & 1 \\ e^{i\phi} & e^{-i\phi} \end{pmatrix}, T_3 = \begin{pmatrix} e^{i\phi} & 1 \\ e^{-i\phi} & e^{i\phi} \end{pmatrix}, \quad (3)$$

where $\phi = 2\pi/3$, $\mathbf{q}_1 = k_\theta(0, -1)$, $\mathbf{q}_2 = k_\theta(\sqrt{3}, 1)/2$, $\mathbf{q}_3 = k_\theta(-\sqrt{3}, 1)/2$, $k_\theta = 2k_D \sin(\theta/2) \approx k_D \theta$ with k_D being the Dirac momentum and w the hopping energy. Estimates based on tight-binding models for AB bilayer graphene suggest that $w \approx 110\text{meV}$, however recent measurements suggest that w might be considerably smaller for some epitaxially grown layers[26].

In the presence of a magnetic field it is convenient to work in the Landau gauge $\mathbf{A} = B(-y, 0)$ and express the Hamiltonian in the representation of the basis states $|Ln\alpha y\rangle$ where $L = 1, 2$ labels the layer, n is the LL index, $\alpha = A, B$ stands for the sub-lattice, and y is the guiding center coordinate. The intra-layer part of the Hamiltonian is diagonal in y , however the T_2 and T_3 inter-layer hopping terms change y by $\pm\Delta$ where $\Delta = \sqrt{3}k_\theta\ell^2/2$. In the presence of a finite B the Hamiltonian therefore describes particles hopping on a set of one-dimensional chains. The Hamiltonian can be block-diagonalized in y by grouping guiding centers separated by integer multiples of Δ (see Supplementary Information).

The guiding center chains become periodic when Φ_0/Φ is rational, allowing a second wave vector to be introduced. The corresponding basis functions are constructed by writing the y -guiding coordinate as $y = y_0 + (mq + j)\Delta$ and Fourier transforming with respect to m . The resulting magnetic Brillouin zone is:

$$\{(k_1, k_2) | 0 < k_1 = y_0/\ell^2 < \Delta/\ell^2, 0 < k_2 < 2\pi/q\Delta\}. \quad (4)$$

The Hamiltonian matrix in this magnetic Bloch representation has dimension $4q$ times the number of Landau levels retained.

We numerically diagonalized the Hamiltonian for various twist angles accounting for inter-Landau level transitions (see Supplementary Information). Because $\alpha \propto \theta^2/B$ the sub-band structure becomes more conspicuous as θ is reduced. On the other hand, the band structure for very small twist angles does not have simple Dirac character even at $B = 0$ [23]. In Fig.1 we show the support of the spectrum for the intermediate case $\theta = 2^\circ$. As the magnetic field is increased (i.e. as α is decreased) all the gaps widen. The terminology of Landau level splitting is useful as long as the single layer Landau levels do not overlap. Mini-gaps as large as 10meV open up within the $n = 0$ Landau level for $B \approx 40\text{T}$. When any one of the three tunneling processes T_j is present alone, the $n = 0$ Landau level splits into two precisely degenerate components. The relatively large gap at the $\nu = 0$ neutrality point which is present over a wide range of α in Fig.1 is a remnant of this behavior which often remains when all three hopping processes are restored.

Since the pioneering work of Thouless *et al.*[5] it has been understood that the Hall conductivity σ_H (in units of e^2/h) is a topological number that must be quantized when the chemical potential lies in an energy gap. Although the support of the spectrum as a function of field has a fractal structure, gaps in the spectra can exist continuously over finite ranges of field. The Landau level filling factors ν at which gaps appear are characterized by two topological integers[5] which satisfy

$$\nu = \sigma_H + s\alpha. \quad (5)$$

Here

$$s = -\frac{\Omega}{A} \left(\frac{\partial N}{\partial \Omega} \right)_B = \frac{\Omega}{A} \frac{\partial^2 \mathcal{F}}{\partial \mu \partial \Omega}, \quad (6)$$

A is the sample's area, Ω is the area of the unit cell, N is the number of electrons in states below that gap, and \mathcal{F} is the grand canonical potential. As a function of ν and α , the Diophantine equation (5) has an infinite number of solutions: $(s, \sigma_H) = (s_0 - mq, \sigma_0 + mp)$ where (s_0, σ_0) is some particular solution and m is any integer. While there is a simple rule to determine s is the classic Hofstadter problem[5] for the moiré butterfly s and σ_H must be determined numerically; for example by plotting the energy gaps as a function of ν and α . The linear dependence assured by equation (5) allows a straightforward identification of σ_H as the intercept of gap lines with the $\alpha = 0$ axis and of s as the gap-line slope. In Fig.2 the energy gaps are plotted for $\theta = 2^\circ$.

Using Fig.2 we can identify the topological quantum numbers for every gap in Fig.1, as illustrated for some of the larger gaps that appear near $\alpha \approx 0.3$. The integers depicted in Fig.1 specify the quantized Hall conductance in the large gaps which appear between $\nu = 1$ and $\nu = -1$. As the electronic density is varied the quantized Hall

conductivity follows the non-monotonic variation $+1, -1, +2, -2, +1, -1$.

As evident from equation (6), in the case of bilayer graphene, the quantum number s can be associated with the chemical potential dependence of a rotational torque. Measurement of this electro-mechanical quantum number presents an interesting challenge to experiment.

Our theory has intriguing consequences for magneto-transport in double-layers grown using chemical vapor deposition (CVD). This type of sample is polycrystalline in nature, characterized by graphene flakes of various sizes that are misoriented relative to one another. A double-layer CVD grown structure will therefore be characterized not by a single twist angle but by a set of θ 's. In the presence of a magnetic field the Hall conductivity of each domain will depend on B and on the particular twist angle of the domain. Because different grains will in general have different Hall conductivities, chiral currents will flow along most grain boundaries.

We note that the considerations presented here do not account for electron-electron interactions[28]. As in the Hofstadter butterfly, fractional quantum Hall states with fractional charge and statistics are possible[29, 30]. The large mini-gaps depicted in Fig.1 and the typical high mobilities of graphene multi-layers are favorable for the experimental observation of these fractional states in exfoliated double-layer graphene samples.

We acknowledge a helpful conversation with João Lopes dos Santos, and thank Gene Mele for pointing out the difference between the moiré pattern and the $T(\mathbf{r})$ periodicity. This work was supported by Welch Foundation grant F1473 and by the NSF-NRI SWAN program.

-
- [1] Harper, P. G., Proc. Phys. Soc. Lon. A **68**, 874 (1955).
 - [2] Azbel', M. Ya., Zh. Eksp. Teor. Fiz. **46**, 939 (1964) [Sov. Phys.-JETP **19**, 634 (1964)].
 - [3] Hofstadter, D. R., Energy levels and wave functions of Bloch electrons in rational and irrational magnetic fields. Phys. Rev. B.**14**, 2239-2249 (1976).
 - [4] Streda, P. Quantised Hall effect in a two-dimensional periodic potential. J. Phys. C: Solid State Phys. **15** L1299-L1303 (1982).
 - [5] Thouless, D. J., Kohomoto, M., Nightingale, M. P., & den Nijs, M. Quantized Hall Conductance in a Two-Dimensional Periodic Potential. Phys. Rev. Lett. **49**, 405-408 (1982).
 - [6] MacDonald, A. H., Landau-level subband structure of electrons on a square lattice. Phys. Rev. B. **28**, 6713-6717 (1983).
 - [7] Gat O., & Avron, J., Magnetic fingerprints of fractal spectra, New J. Phys. **5**, 44.1-44.8 (2003).
 - [8] Amidror, I. The Theory of the Moire Phenomenon Vol. I (Springer, London 2009).

- [9] MacDonald, A. H., Quantized Hall effect in a hexagonal periodic potential. *Phys. Rev. B.* **26**, 3057-3065 (1984).
- [10] MacDonald, A. H. *Physique Quantique Méscopique*, Les Houches Session LXI, edited by E. Akkermans et al. (Elsevier, Amsterdam, 1995).
- [11] Albrecht, C., Smet, J. H., von Klitzing K., Weiss, D., Umansky, V., & Schweizer, H., Evidence of Hofstadters Fractal Energy Spectrum in the Quantized Hall Conductance. *Phys. Rev. Lett.* **86**, 147-150 (2001).
- [12] Rong, Z. Y. & Kuiper, P. Electronic effects in scanning tunneling microscopy: Moiré pattern on a graphite surface. *Phys. Rev. B* **48**, 17427-17431 (1993).
- [13] Hass, J., Varchon, F., Milln-Otoya, J. E., Sprinkle, M., Sharma, N., de Heer, W. A., Berger, C., First, P. N., Magaud, L., & Conrad E. H. Why Multilayer Graphene on 4H-SiC(000 $\bar{1}$) Behaves Like a Single Sheet of Graphene. *Phys. Rev. Lett.* **100**, 125504 (2008).
- [14] Luican, A., Li, G., Reina, A., Kong, J., Nair, R. R., Novoselov, K. S., Geim, A. K., & Andrei E.Y. Single Layer Behavior and Its Breakdown in Twisted Graphene Layers. arXiv:1010.4032.
- [15] Schmidt, H., Luedtke, T., Barthold, P. & Haug, R. J. Mobilities and scattering times in decoupled graphene monolayers. *Phys. Rev. B* **81**, 121403(R) (2010).
- [16] Kwanpyo, K., Lee, Z., Malone, B., Chan, K. T., Regan, W., Gannett, W., Alemn, B., Crommie, M. F., Cohen, M. L., & Zettl, A. Multiply Folded Graphene: Grafold. arXiv:1012.5426.
- [17] Lopes dos Santos, J. M. B., Peres, N. M. R., & Castro Neto, A. H. Graphene Bilayer with a Twist: Electronic Structure. *Phys. Rev. Lett.* **99**, 256802 (2007).
- [18] Shallcross, S., Sharma, S., Kandelaki, E., & Pankratov, O. A. Electronic structure of turbostratic graphene. *Phys. Rev. B* **81**, 165105 (2010).
- [19] Trambly de Laissardie're, G., Mayou, D., & Magaud, L. Localization of Dirac Electrons in Rotated Graphene Bilayers. *Nano Lett.* **10**, 804-808 (2010).
- [20] Morell, E. S., Correa, J. D., Vargas, P., Pacheco, M., & Barticevic, Z. Flat bands in slightly twisted bilayer graphene: Tight-binding calculations. *Phys. Rev. B* **82**, 121407(R) (2010).
- [21] Mele, E. J. Commensuration and interlayer coherence in twisted bilayer graphene. *Phys. Rev. B* **81**, 161405(R) (2010).
- [22] Bistritzer, R., & MacDonald, A. H. Transport between twisted graphene layers. *Phys. Rev. B* **81**, 245412 (2010).
- [23] Bistritzer, R., & MacDonald, A. H. Moiré bands in twisted double-layer graphene. arXiv:1009.4203.
- [24] Li, G., Luican, A., Lopes dos Santos, J. M. B., Castro Neto, A. H., Reina, A., Kong, J., & Andrei, E. Y. Observation of Van Hove singularities in twisted graphene layers. *Nature Phys.* **6**, 109-113 (2010).
- [25] Novoselov, K. S., Jiang, Z., Zhang, Y., Morozov, S. V., Stormer, H. L., Zeitler, U., Maan, J. C., Boebinger, G. S., Kim, P., & Geim A. K. Room-Temperature Quantum Hall Effect in Graphene. *Science* **315**, 1379 (2007).
- [26] Hicks, J., Sprinkle, M., Shepperd, K., Wang, F., Tejada, A., Taleb-Ibrahimi, A., Bertran, F., Le Fvre, P., de Heer, W.A.,

- Berger, C., & Conrad E.H. Symmetry breaking in commensurate graphene rotational stacking; a comparison of theory and experiment. arXiv:1012.0460.
- [27] Dana, I., Avron, Y., & Zak, J., Quantised Hall conductance in a perfect crystal. *J. Phys. C: Solid State Phys.* **18** (1985) L679-L683.
- [28] Avron, J. E., & Yaffe, L. G. Diophantine Equation for the Hall Conductance of Interacting Electrons on a Torus. *Phys. Rev. Lett.* **56**, 2084-2087 (1986).
- [29] Kol, A., & Read, N. Fractional quantum Hall effect in a periodic potential. *Phys. Rev. B.* **48**, 8890 (1993).
- [30] Pfannkuche, D., & MacDonald, A. H. Quantum Hall effect of interacting electrons in a periodic potential. *Phys. Rev. B.* **56**, R7100-R7103 (1997).
- [31] MacDonald, A. H., Influence of Landau level mixing on the charge-density-wave state of a two-dimensional electron gas in a strong magnetic field. *Phys. Rev. B.* **30**, 4392-4398 (1984).
- [32] Geisler, M. C., Smet, J. H., Umansky, V., von Klitzing, K., Naundorf, B., Ketzmerick, R., & Schweizer, H., Detection of a Landau Band-Coupling-Induced Rearrangement of the Hofstadter Butterfly. *Phys. Rev. Lett.* **92**, 256801 (2004).

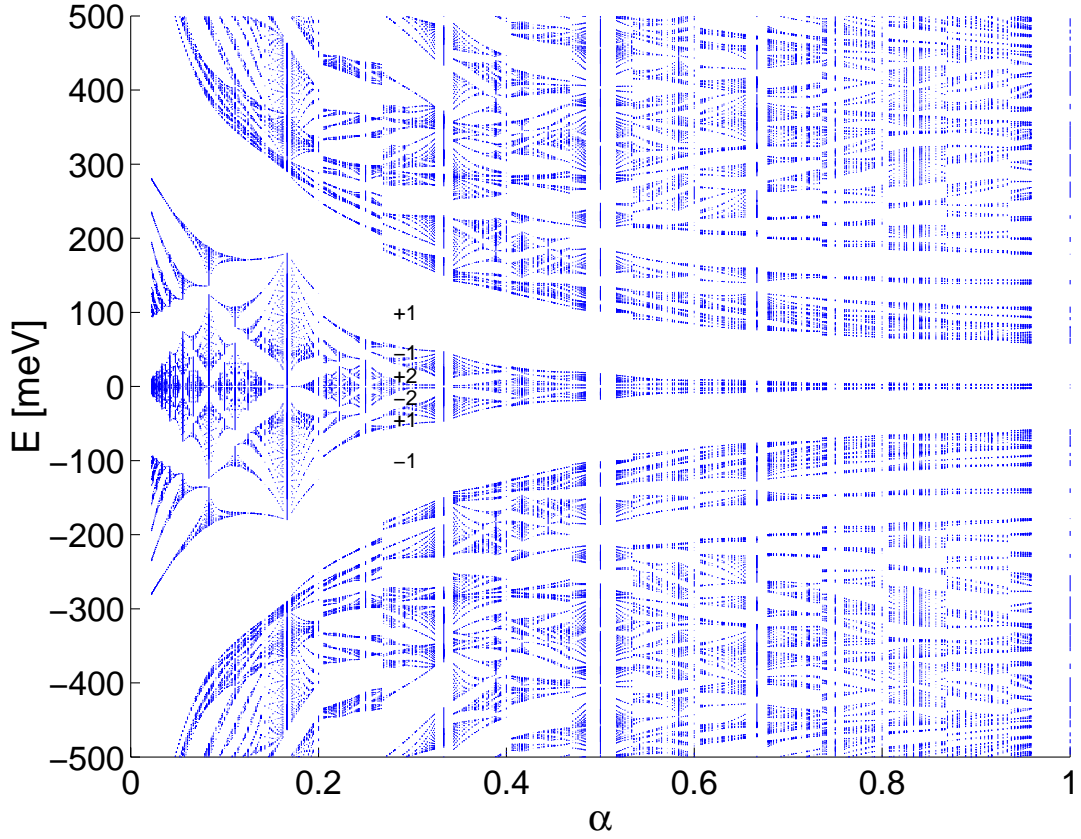


FIG. 1: **Spectrum support.** The support of the spectrum as a function of α for $\theta = 2^\circ$ ($w = 110\text{meV}$). The periodic inter-layer hopping amplitude results in a Hofstadter-like sub-band structure. The integers denote the Hall conductivity associated with the larger energy gaps between $\nu = 1$ and $\nu = -1$ for $\alpha \approx 0.3$.

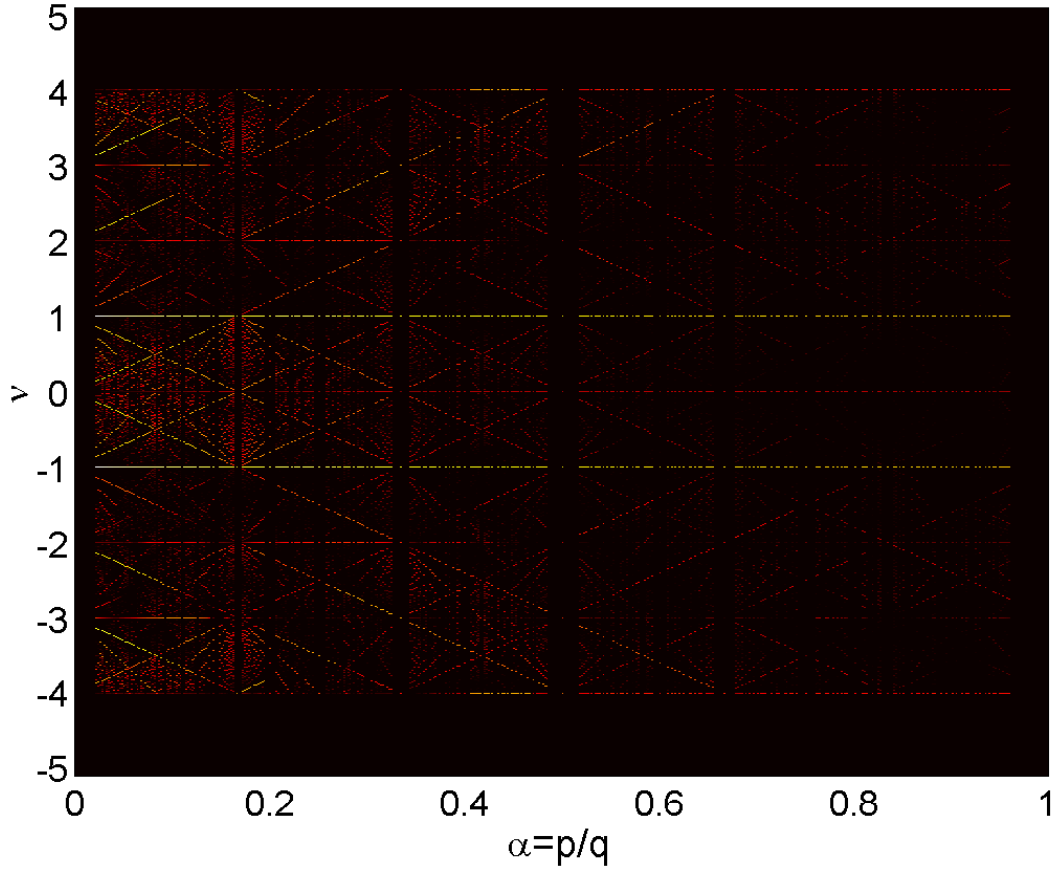


FIG. 2: **Hall conductivity.** A color plot for the energy gaps as a function of filling factor ν and p/q for $\theta = 2^\circ$ ($w = 110\text{meV}$). The color scale corresponds to $\log(1 + \text{gap})$ in order to magnify the smaller gaps. The conspicuous straight lines satisfy the Diophantine gap equation (5) and determine both σ_H and s . The Hall conductivity corresponds to the intercept of the line with the y-axis whereas s is given by its slope.

Supplementary Information

HAMILTONIAN

To find the spectrum of the Hamiltonian given by equation (1) we represent it in terms of the basis states $|Ln\alpha y\rangle$ where $L = 1, 2$ labels the layer, n is the Landau level index, $\alpha = A, B$ stands for the sub-lattice and y is the guiding center coordinate. The intra-layer part of the Hamiltonian is then

$$h(\theta) = -\omega_c \sum_{Ln y} (e^{-i\theta} \sqrt{n+1} |Ln+1Ay\rangle \langle LnBy| + h.c.), \quad (7)$$

and the inter-layer part is

$$T = \sum_{nmy\alpha\beta} \left(T^{(0)} |2n\alpha y\rangle \langle 1m\beta y| + T^{(R)} |2n\alpha y + \Delta\rangle \langle 1m\beta y| + T^{(L)} |2n\alpha y - \Delta\rangle \langle 1m\beta y| \right). \quad (8)$$

Here $\Delta = \frac{\sqrt{3}}{2} k_\theta \ell^2$,

$$\begin{aligned} T^{(0)} &= T_1 F_{nm} \left(\frac{\mathbf{q}_1 \ell}{\sqrt{2}} \right) e^{-ik_\theta y} \\ T^{(R)} &= T_2 F_{nm} \left(\frac{\mathbf{q}_2 \ell}{\sqrt{2}} \right) e^{\frac{i}{4} k_\theta (2y - \Delta)} \\ T^{(L)} &= T_3 F_{nm} \left(\frac{\mathbf{q}_3 \ell}{\sqrt{2}} \right) e^{\frac{i}{4} k_\theta (2y + \Delta)}, \end{aligned} \quad (9)$$

(the T_j 's are defined by equation (3) in the main text) and

$$F_{nm}(\mathbf{z}) = \sqrt{\frac{m!}{n!}} (-z_x + iz_y)^{n-m} e^{-\frac{z^2}{2}} \mathcal{L}_m^{n-m}(z^2) \quad (10)$$

for $n \geq m$ with \mathcal{L} being the associated Laguarre polynomial. For $n < m$ the function F can be found using $F_{nm}(\mathbf{z}) = F_{mn}^*(-\mathbf{z})$.

The commensurability condition $p/q = \Phi_0/\Omega_M B$ is equivalent to the condition $k_\theta \Delta/2 = 2\pi p/q$ for which the hopping amplitudes (9) repeat their values when y is shifted by $q\Delta$. As explained in the main text, this last periodicity together with the y_0 guiding center coordinate define a magnetic Brillouin zone. For each momentum $\mathbf{k} = (k_1, k_2 = y_0/\ell^2)$ in that zone

$$T(\mathbf{k}) = \sum_{n\alpha\beta j} \left[T_j^{(0)} |2n\alpha j\rangle \langle 1m\beta j| + T_j^{(R)} |2n\alpha, j+1\rangle \langle 1m\beta j| + T_j^{(L)} |2n\alpha j-1\rangle \langle 1m\beta j| \right], \quad (11)$$

where $j = 0, 1, \dots, q-1$ (j is defined modulo q so that $|j = q\rangle = |j = 0\rangle$), and

$$\begin{aligned} T_j^{(0)} &= T_1 F_{nm} \left(\frac{\mathbf{q1}\ell}{\sqrt{2}} \right) e^{-ik_\theta y_0} e^{-4\pi i \frac{p}{q} j} \\ T_j^{(R)} &= T_2 F_{nm} \left(\frac{\mathbf{q2}\ell}{\sqrt{2}} \right) e^{ik_2 \Delta} e^{\frac{i}{2} k_\theta y_0} e^{i\pi \frac{p}{q} (2j-1)} \\ T_j^{(L)} &= T_3 F_{nm} \left(\frac{\mathbf{q3}\ell}{\sqrt{2}} \right) e^{-ik_2 \Delta} e^{\frac{i}{2} k_\theta y_0} e^{i\pi \frac{p}{q} (2j+1)}. \end{aligned} \quad (12)$$

Because $(k_\theta \ell)^2 = 8\pi p / \sqrt{3} q$, the inter-layer Hamiltonian depends only on p/q . In the absence of Landau level mixing the splitting of each Landau level into sub-bands is therefore determined only by α .

Inter-Landau level transitions can significantly alter the electronic spectrum[31, 32]. In the absence of a magnetic field two momentum states are effectively coupled if their energy difference is of order of $E_\Lambda = \max(vk_\theta, w)$ or less. The same criteria holds also in the presence of a magnetic field. The $n = 0$ Landau level therefore couples most strongly to the $n_0 \approx (E_\Lambda / \omega_c)^2$ Landau level. In our calculations we retain $2n_0$ Landau levels in order to obtain spectra that are accurate near the Dirac point. Comparing Fig.1 with results obtained neglecting Landau level mixing (not shown) we find that, as expected, inter-Landau level hopping is increasingly important as the magnetic field is reduced and as the energy is increased.

A naive approach to implement an energy cutoff would be to keep all states whose Landau level index is less than $2n_0$. The problem with this approach is that it introduces a fake zero energy state irrespective of the size of n_0 . We therefore make the energy cutoff such that only one sub-lattice of the n_0 Landau level is retained. This approach shifts the numerical error to high energies, of the order of $\sqrt{n_0} \omega_c$.

MOIRÉ UNIT CELL

The inter-layer hopping in twisted double layer graphene is akin in some respects to a periodic potential. In a real space representation it is described by the 4×4 matrix (layer \times sub-lattice)

$$H_{\mathbf{r}} = \begin{pmatrix} 0 & T(\mathbf{r}) \\ T^\dagger(\mathbf{r}) & 0 \end{pmatrix} \quad (13)$$

where $T(\mathbf{r})$ is given by equation (2) in the main text. The AA entry of the T -matrix is depicted in Fig.3 (similar figures are obtained for the other entries of T). The direction and size of an arrow at point \mathbf{r} correspond, respectively to the phase of $T_{AA}(\mathbf{r})$ and to its magnitude. The red dots mark the lattice associated with the moiré pattern whereas

the green circles mark the lattice induced by $T(\mathbf{r})$. Interestingly, the moiré unit cell area

$$\Omega_M = 16\pi^2/\sqrt{3}k_\theta^2 \quad (14)$$

is six times larger than the area of the moiré pattern unit cell[23].

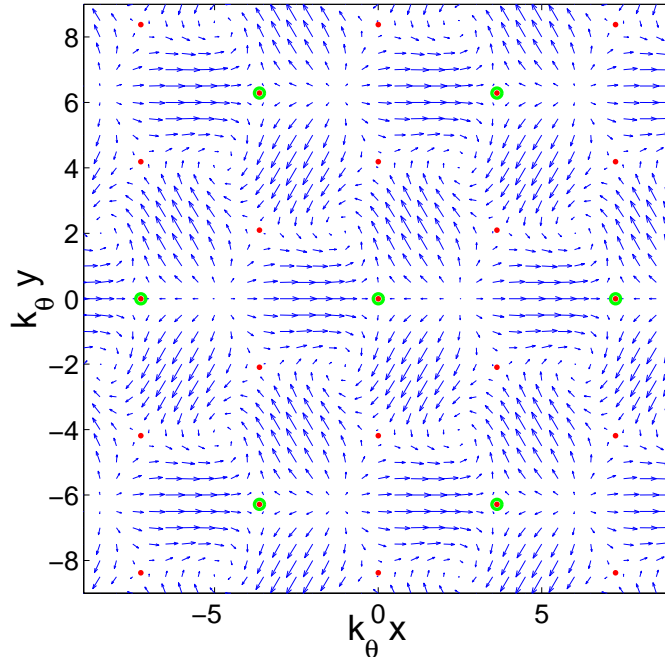


FIG. 3: **Moiré unit cell.** The AA entry of the hopping amplitude is plotted as a function of position (in units of k_θ^{-1}). The space dependent eigenvalues of H_T lead to the moiré pattern period marked by the red dots, however the spatial variation of the phase of T results in a larger period denoted by the green circles. It is this latter periodicity that determines the moiré unit cell area Ω_M .